A Mixed-Enhanced Strain Method: Linear Problems

Eric P. Kasper[1] and Robert L. Taylor[1]

[1]Department of Civil and Environmental Engineering
University of California at Berkeley, Berkeley, CA 94720-1710

Report No.: UCB/SEMM-97/02

Abstract

A general formulation of an assumed strain method in the context of mixed finite elements is presented. A mixed strain field is presented to which an enhancement is added resulting in a formulation which produces coarse mesh accuracy in bending dominated problems and locking-free response in the near incompressible limit. The structure of the mixed fields present permits a consistent variational stress recovery. Also, the construction of the formulation is such that the mixed parameters may be obtained explicitly and the resulting finite element arrays obtain full rank using standard order quadrature. In this paper our attention is restricted to the area of geometrically linear problems in solid mechanics. Specifically, we investigate the proposed formulation in the setting of nearly incompressible elasticity, physically nonlinear plasticity and thin shell structures. Representative simulations show favorable performance of the formulation.

1. Introduction

It is known that finite elements based upon low order isoparametric displacement formulations exhibit poor performance in bending and locking in the nearly incompressible limit. Recent formulations which exhibit improved accuracy with respect to these two deficiencies fall into two categories namely *assumed stress* and *assumed strain* methods. The formulation presented herein is addressed in the context of *assumed strain* methods which have been preferred to their *assumed stress* counterparts, due to their natural compatibility with the strain drive format typically found in the algorithmic development of nonlinear materials.

One of the first developments in the area of *assumed strain* methods was by Wilson *et al.*, [1973] who proposed the addition of internal incompatible displacement modes of quadratic distribution to enhance bending performance of quadrilateral elements. Subsequently, it was discovered that the element failed the patch test for an arbitrary quadrilateral. Taylor *et al.*, [1976] proposed modifications to Wilson's original formulation which allowed for satisfaction of the patch test for arbitrary configurations. In later developments Simo & Rifai, [1990] present a systematic development of a class of *assumed strain* methods. They provided the framework for the development of low order elements possessing improved performance in bending dominate problems in the context of small strains. Issues related to convergence and stability were also presented. Further extensions were made to incorporate geometrically nonlinearities by Simo & Armero, [1992], but was found to lock in the incompressible limit for three dimensional hexagonal elements for both geometrically linear and nonlinear problems. Improvements were made for the three dimensional formulation by Simo *et al.*, [1993] which incorporated modifications to the tri-linear shape functions, additional enhanced modes and an increased quadrature rule. The resulting element yielded a locking-free response in the incompressible limit and improved bending characteristics for both geometrically linear and nonlinear problems. ANDELFINGER *et al.*, [1992] developed two and three dimensional enhanced strain elements for linear kinematics which overcome locking in the incompressible limit and behaved well in bending dominated regimes, but required a minimum of 21 element parameters for three dimensions. WEISSMAN, [1996] also presented an enhanced formulation based on a three field functional which yield good performance for a wide class of problems using 15 element parameters. More recently, KORELC & WRIGGERS, [1996], [1997] developed two and three dimensional enhanced strain elements which yield favorable results, with only 9 element parameters, thereby improving the efficiency of the element.

The approach of the present work utilizes a mixed finite element technique to overcome the difficulties which arise in the near incompressible limit and simultaneously enhance the resulting mixed strain field to improve coarse mesh accuracy in bending. Also, the formulation maintains a strain drive format such that general constitutive equations can be treated identically as in the Galerkin displacement finite element method. The approach is set forth by a reparametrization of the strain field in terms of a mixed approximation, from which a consistent formulation is derived. An additional enhancement is made to the strain field to improve the bending characteristics and give a locking-free response. The formulation is shown to have the appropriate convergence conditions as set forth in SIMO & RIFAI, [1990], namely consistency and stability. The element is formulated such that only standard order quadrature is needed for full rank, while maintaining a minimum number of element parameters, to achieve accurate results. The formulation also circumvents difficulties which can arise in *assumed strain* methods, for variational stress recovery.

The formulation of the strain field which appears in SIMO & RIFAI and others differs from the present work in the reparametrization of the strain field. As a consequence of their formulations, orthogonality conditions arise explicitly between the stress and enhanced strain field. This orthogonality condition makes full variational stress recovery difficult, if not impossible. The same orthogonality constraint exists implicitly in the present formulation, but due to the mixed construction of the stress field variational stress recovery is permissible.

The paper is outlined as follows. In §2, basic notation is given as well as the variational formulation for the model which is then cast into its weak form. Finite element interpolations are introduced in §3 along with the transformation relations for the mixed fields. The mixed-enhanced strain field and variationally consistent stress field recovery are developed and presented. The residual equations are then obtained from which a numerical formulation is presented. Representative numerical simulations for the case of plane strain and three dimensional elasticity are presented in §4, for linear kinematics with either elastic or elastic-plastic constitutive equations. Finally, in §5 conclusions are drawn and further work outlined.

2. Mixed-Enhanced Strain Formulation

This section examines the proposed formulation in the setting of linear elasticity. We begin with an introduction of the basic notation used and then summarize a three-field Hu-Washizu functional in which the Dirichlet condition $\boldsymbol{u} = \overline{\boldsymbol{u}}$ on Γ_u is explicitly enforced. Finally, we present the resulting field equations in the weak form which is used subsequently for the finite element formulation.

2.1. Notation

The open set $\Omega \subset \mathrm{R}^n (n = 1, 2 \ or \ 3)$ with smooth boundary $\partial\Omega$ represents a bounded reference configuration $\mathcal{B}$ for the continuum body. We admit the decomposition of the boundary into two parts: $\Gamma_u \subset \partial\Omega$ where the displacement is prescribed as $\boldsymbol{u} = \overline{\boldsymbol{u}}$ and $\Gamma_t \subset \partial\Omega$ where the traction vector is prescribed as $\overline{\boldsymbol{t}} = \boldsymbol{\sigma}\boldsymbol{n}$ subject to

$$\partial\Omega = \overline{\Gamma_u \cup \Gamma_t} \quad \text{and} \quad \Gamma_u \cap \Gamma_t = \emptyset \tag{2.1}$$

where $\boldsymbol{\sigma}$ is the stress tensor and $\boldsymbol{n}$ is the outward normal to the boundary.

The governing equations for linear elastostatics are given by the balance of linear and angular momentum

$$\begin{aligned} \mathrm{Div}\,[\boldsymbol{\sigma}] + \boldsymbol{b} &= \boldsymbol{0} \\ \boldsymbol{\sigma} &= \boldsymbol{\sigma}^T \end{aligned} \tag{2.2}$$

the strain-displacement relationship

$$\boldsymbol{\varepsilon} = \nabla^{(s)}\boldsymbol{u} = \frac{1}{2}\left(\nabla\boldsymbol{u} + \nabla\boldsymbol{u}^T\right) \tag{2.3}$$

and for elastic stress response the constitutive equations

$$\boldsymbol{\sigma} = \frac{\partial W}{\partial \boldsymbol{\varepsilon}} \ . \tag{2.4}$$

In the above $\boldsymbol{\varepsilon}$ denotes the infinitesimal strain tensor, $\boldsymbol{\sigma}$ the stress tensor, $W(\boldsymbol{X}, \boldsymbol{\varepsilon})$ is a convex stored energy function, $\boldsymbol{b}$ is the body force per unit volume and $\mathrm{Div}\,[\cdot]$ is the divergence operator.

For subsequent development let $\mathcal{U}$ be the space of admissible displacements written as

$$\mathcal{U} = \left\{\boldsymbol{u} : \Omega \to \mathrm{R}^n \mid \boldsymbol{u} \in H^1(\Omega) \text{ and } \boldsymbol{u} = \overline{\boldsymbol{u}} \text{ on } \Gamma_u\right\} \tag{2.5}$$

while the space of admissible stresses and strains are denoted by $\mathcal{M}$

$$\mathcal{M} = \left\{\boldsymbol{h} : \Omega \to \mathrm{R}^n \times \mathrm{R}^n \mid h_{ij} \in L^2(\Omega)\right\} \ . \tag{2.6}$$

2.2. Variational Formulation

An approximate solution of the boundary value problem is constructed from a variational statement of the problem. The basic field equations may be included in a variational statement for the elasticity problem using a Hu-Washizu functional, WASHIZU, [1982]. We use a special case of one such functional and examine its implications. Accordingly, we have a functional in which the displacement field, $\boldsymbol{u} \in \mathcal{U}$, the stress tensor, $\tilde{\boldsymbol{\sigma}} \in \mathcal{M}$ and the strain tensor, $\tilde{\boldsymbol{\varepsilon}} \in \mathcal{M}$ are regarded as the independent variables. The proposed three-field functional $\Pi : \mathcal{U} \times \mathcal{M} \times \mathcal{M} \to \mathrm{R}$ may be expressed as

$$\Pi(\boldsymbol{u}, \tilde{\boldsymbol{\varepsilon}}, \tilde{\boldsymbol{\sigma}}) = \int_\Omega \left[W(\boldsymbol{X}, \tilde{\boldsymbol{\varepsilon}}) + \tilde{\boldsymbol{\sigma}} : (\boldsymbol{\varepsilon} - \tilde{\boldsymbol{\varepsilon}}) \right] \, dV \; + \; \Pi_{ext}(\boldsymbol{u}) \tag{2.7}$$

where for conservative external loading

$$\Pi_{ext}(\boldsymbol{u}) = - \int_\Omega \boldsymbol{b} \cdot \boldsymbol{u} \, dV - \int_{\Gamma_t} \bar{\boldsymbol{t}} \cdot \boldsymbol{u} \, dS \; . \tag{2.8}$$

We may state the solution of (2.7) as: Find the $\boldsymbol{u}$, $\tilde{\boldsymbol{\varepsilon}}$ and $\tilde{\boldsymbol{\sigma}}$, with $\boldsymbol{u}$ satisfying the Dirichlet boundary condition $\boldsymbol{u} = \bar{\boldsymbol{u}}$ on Γ_u, which make the Hu-Washizu functional $\Pi(\boldsymbol{u}, \tilde{\boldsymbol{\varepsilon}}, \tilde{\boldsymbol{\sigma}})$ stationary for all admissible variations $\delta \boldsymbol{u} \in \mathcal{V}$, $\delta \tilde{\boldsymbol{\varepsilon}} \in \mathcal{M}$ and $\delta \tilde{\boldsymbol{\sigma}} \in \mathcal{M}$. Where $\mathcal{V}$ is the space of admissible variations in the displacement written as

$$\mathcal{V} = \left\{ \delta \boldsymbol{u} : \Omega \to \mathrm{R}^n \mid \delta \boldsymbol{u} \in H^1(\Omega) \text{ and } \delta \boldsymbol{u} = \boldsymbol{0} \text{ on } \Gamma_u \right\} \; . \tag{2.9}$$

Since there are no explicit constraints on $\tilde{\boldsymbol{\varepsilon}}$ and $\tilde{\boldsymbol{\sigma}}$ we may take the variations $\delta \tilde{\boldsymbol{\varepsilon}}$ and $\delta \tilde{\boldsymbol{\sigma}}$ to be contained within $\mathcal{M}$ as defined in (2.6).

The stationary point of Π is obtained by setting to zero the first variation of (2.7) with respect to the three independent fields. Accordingly

$$\begin{aligned} \int_\Omega \delta \boldsymbol{\varepsilon} \cdot \tilde{\boldsymbol{\sigma}} \, dV - \int_\Omega \delta \boldsymbol{u} \cdot \boldsymbol{b} \, dV - \int_{\Gamma_t} \delta \boldsymbol{u} \cdot \bar{\boldsymbol{t}} \, dS &= 0 \\ \int_\Omega \delta \tilde{\boldsymbol{\varepsilon}} \cdot \left(\frac{\partial W}{\partial \tilde{\boldsymbol{\varepsilon}}} - \tilde{\boldsymbol{\sigma}} \right) \, dV &= 0 \qquad \text{in } \Omega \\ \int_\Omega \delta \tilde{\boldsymbol{\sigma}} \cdot (\boldsymbol{\varepsilon} - \tilde{\boldsymbol{\varepsilon}}) \, dV &= 0 \; . \end{aligned} \tag{2.10}$$

for all admissible variations $\delta \boldsymbol{u} \in \mathcal{V}$, $\delta \tilde{\boldsymbol{\varepsilon}} \in \mathcal{M}$ and $\delta \tilde{\boldsymbol{\sigma}} \in \mathcal{M}$.

3. Finite Element Approximations

In this section we outline the interpolates used for the field variables, from which the mixed strain and stress fields are constructed in terms of nodal parameters as well as internal element parameters. Using the mixed strain field we construct an approximation to the three-field variational formulation. We then use the stationary condition to yield a reduced set of nonlinear equations, which are then linearized. From these equations finite element arrays are formulated. Finally, we outline a procedure for implementation of the formulation.

3.1. Finite Element Interpolations for the Field Variables

We begin by a discretization of the given reference domain Ω into a collection of polygonal shaped subdomains, $\bar{\Omega}_e$ such that $\Omega \approx \Omega^h = \bigcup_e \bar{\Omega}_e$ where $\bar{\Omega}_e$ is the closure of an individual element. Note that the collection is an approximation of the actual domain Ω. We admit the decomposition of the approximation to the boundary as $\partial\Omega \approx \partial\Omega^h = \overline{\Gamma_u^h \cap \Gamma_t^h}$ and $\Gamma_u^h \cup \Gamma_t^h = \emptyset$.

For isoparametric finite elements we define the reference geometry $\mathbf{X}^h \in \mathrm{R}^n$ and displacement field $\mathbf{u}^h \in \mathcal{U}^h$ over a typical element $\bar{\Omega}_e$ in the form

$$\mathbf{X}^h = \sum_{I=1}^{nen} N_I(\boldsymbol{\xi})\, \widehat{\mathbf{X}}^I \quad \text{and} \quad \mathbf{u}^h = \sum_{I=1}^{nen} N_I(\boldsymbol{\xi})\, \widehat{\mathbf{u}}^I\ , \tag{3.1}$$

where $N_I(\boldsymbol{\xi})$ are the standard isoparametric shape functions associated with node I, nen is the number of nodes on element $\bar{\Omega}_e$, h is a characteristic length of element $\bar{\Omega}_e$ and $\widehat{\mathbf{u}}^h, \widehat{\mathbf{X}}^h \in \mathrm{R}^n$, see Zienkiewicz & Taylor, [1989] or Hughes, [1987] for further details.

For the approximate problem we introduce the space $\mathcal{U}^h$ as a finite-dimensional approximation of $\mathcal{U}$, accordingly the space of admissible displacement fields maybe written as

$$\mathcal{U}^h = \left\{ \mathbf{u}^h \mid \mathbf{u}^h \in H^1(\Omega^h) \text{ and } \mathbf{u}^h = \bar{\mathbf{u}}^h \text{ on } \Gamma_u^h \right\}\ . \tag{3.2}$$

Lastly, the space $\mathcal{M}^h$, which contains the approximations to the stress and strain fields, is a finite-dimensional approximation of $\mathcal{M}$ given by

$$\mathcal{M}^h = \left\{ \boldsymbol{h}^h \mid h_{ij}^h \in L^2(\Omega^h) \right\}\ . \tag{3.3}$$

3.1.1. Mixed Quantities.

The key idea for the mixed stress and strain fields is to develop the interpolates in the natural or isoparametric space and transform the results to the physical space. Based on requirements of tensor calculus, Sokolnikoff, [1964], we use the following transformation relations for the stress and strain tensors

$$\mathcal{S}_{\alpha\beta}(\boldsymbol{\xi}, \boldsymbol{\beta}) = \tilde{\boldsymbol{\sigma}}_{IJ}(\boldsymbol{T}_{I\alpha})^{-1}(\boldsymbol{T}_{J\beta})^{-1} \quad \text{and} \quad \mathcal{E}_{\alpha\beta}(\boldsymbol{\xi}, \boldsymbol{\beta}) = \tilde{\boldsymbol{\varepsilon}}_{IJ}\boldsymbol{T}_{I\alpha}\boldsymbol{T}_{J\beta} \tag{3.4}$$

where $\mathcal{S}$ and $\mathcal{E}$ are the stress and strain in the isoparametric space, respectively. The above are defined so that $\mathcal{S} : \mathcal{E} = \tilde{\boldsymbol{\sigma}} : \tilde{\boldsymbol{\varepsilon}}$.

Let $\square$ denote the parent domain in the isoparametric space $\boldsymbol{\xi}$. Utilizing the mapping $\boldsymbol{X} : \square \to \Omega_e$ the Jacobian is expressed as

$$J_{I\alpha}(\boldsymbol{\xi}) = \frac{\partial X^I}{\partial \xi^\alpha}\ . \tag{3.5}$$

For the present paper the Jacobian used in (3.4) is averaged over the element Ω_e and used to define $\boldsymbol{T}$. This will permit direct inclusion of constant states, minimize the order of quadrature needed to evaluate the residual and tangent arrays and also eliminate problems associated with initially distorted elements. The average is denoted as

$$\boldsymbol{T} = \frac{1}{\Omega_e} \int_{\Omega_e} \boldsymbol{J}(\boldsymbol{\xi}) \; dV \; . \tag{3.6}$$

Substituting (3.6) into (3.4) yields the transformation of the fields $(\mathcal{S}, \mathcal{E})$ in the isoparametric space to the fields $(\tilde{\boldsymbol{\sigma}}, \tilde{\varepsilon})$ in the physical space

$$\mathcal{S}(\boldsymbol{\xi}, \boldsymbol{\beta}) = \boldsymbol{T}^{-1} \tilde{\boldsymbol{\sigma}} \boldsymbol{T}^{-T} \quad \text{and} \quad \mathcal{E}(\boldsymbol{\xi}, \gamma) = \boldsymbol{T}^{T} \tilde{\varepsilon} \boldsymbol{T} \; . \tag{3.7}$$

Remark 3.1.

1. Alternatively, the Jacobian can be evaluated at the centroid, as originally suggested by Pian & Sumihara, [1985] and Taylor *et al.*, [1976]. Note for two dimensions the average and centroidal Jacobians are identical.
2. Since the above transformation relations for the stress and strain are typically a measure of the isoparametric and physical space alternative transformations are admissible. Numerical observation by Glaser & Armero, [1996] and Wriggers & Reese, [1996] and confirmed during the developments of the present work show that replacing $\boldsymbol{J}$ by $\boldsymbol{J}^{-T}$ result in transformation relations which are superior for the class of problems examined.

We assume there exist linear maps $\mathcal{E}_1(\boldsymbol{\xi}, \cdot)$ and $\mathcal{E}_2(\boldsymbol{\xi}, \cdot)$ for which the fields $(\mathcal{S}, \mathcal{E})$ in the isoparametric space may be expressed as:

$$\begin{aligned} \mathcal{S}(\boldsymbol{\xi}, \boldsymbol{\beta}) &= \widehat{\boldsymbol{\beta}}_0 + \mathcal{E}_1(\boldsymbol{\xi}, \boldsymbol{\beta}) \\ \mathcal{E}(\boldsymbol{\xi}, \gamma) &= \widehat{\gamma}_0 + \frac{1}{j} \left[\mathcal{E}_1(\boldsymbol{\xi}, \gamma) + \mathcal{E}_2(\boldsymbol{\xi}, \boldsymbol{\alpha}) \right] \end{aligned} \tag{3.8}$$

where $\widehat{\boldsymbol{\beta}}_0$, $\boldsymbol{\beta}$, $\widehat{\gamma}_0$ and $\boldsymbol{\gamma}$ are parameters and $\mathcal{E}_1(\boldsymbol{\xi}, \gamma)$ and $\mathcal{E}_2(\boldsymbol{\xi}, \boldsymbol{\alpha})$ denote linear forms

$$\mathcal{E}_1(\boldsymbol{\xi}, \gamma) = \sum_{k=1}^{n} \mathcal{E}_{k1}(\boldsymbol{\xi}) \gamma_k \quad \text{and} \quad \mathcal{E}_2(\boldsymbol{\xi}, \boldsymbol{\alpha}) = \sum_{k=1}^{m} \mathcal{E}_{k2}(\boldsymbol{\xi}) \boldsymbol{\alpha}_k$$

where n and m are the number of parameters for the mixed and enhanced fields, respectively.

We construct the approximations $\mathcal{E}_1$ and $\mathcal{E}_2$ such that

$$\int_{\square} \mathcal{E}_1(\cdot) \; d\square = 0 \; , \quad \int_{\square} \mathcal{E}_2(\cdot) \; d\square = 0 \quad \text{and} \quad \int_{\square} \mathcal{E}_1(\cdot) \mathcal{E}_2(\cdot) \; d\square = 0 \; . \tag{3.9}$$

The relations in (3.9) will be used subsequently to decouple and solve for the element parameters of the mixed stress and strain.

Remark 3.2.

1. The mapping $\mathcal{E}_2(\boldsymbol{\xi}, \boldsymbol{\alpha})$ with its associated element parameters, $\boldsymbol{\alpha}$ were added to $(3.8)_2$ for two reasons: a) to improve performance in nearly incompressible regions, b) and to improve coarse mesh accuracy in bending dominated regimes.
2. Note the strain field in (3.8) has more parameters than the stress, hence we adopt the phrase *mixed-enhanced strain* as an extension of the terminology introduced by Simo & Rifai, [1990].

For two and three dimensional problems employing 4-node quadrilateral and 8-node hexahedral elements the maps $\mathcal{E}_1(\boldsymbol{\xi}, \cdot)$ and $\mathcal{E}_2(\boldsymbol{\xi}, \cdot)$ are given in Tables 3.1 and 3.2 below, respectively. Noting symmetry the independent components are ordered in standard Voigt notation as:

Table 3.1 Two Dimensional Interpolations

i	j	$[\mathcal{E}_1(\boldsymbol{\xi}, \boldsymbol{\gamma})]_{ij}$	$[\mathcal{E}_2(\boldsymbol{\xi}, \boldsymbol{\alpha})]_{ij}$
1	1	$\xi_2\gamma_1$	$\xi_1\alpha_1$
2	2	$\xi_1\gamma_2$	$\xi_2\alpha_2$
1	2	0	0

Table 3.2 Three Dimensional Interpolations

i	j	$[\mathcal{E}_1(\boldsymbol{\xi}, \boldsymbol{\gamma})]_{ij}$	$[\mathcal{E}_2(\boldsymbol{\xi}, \boldsymbol{\alpha})]_{ij}$
1	1	$\xi_2\gamma_1 + \xi_3\gamma_2 + \xi_2\xi_3\gamma_3$	$\xi_1\alpha_1 + \xi_1\xi_2\alpha_2 + \xi_1\xi_3\alpha_3$
2	2	$\xi_1\gamma_4 + \xi_3\gamma_5 + \xi_1\xi_3\gamma_6$	$\xi_2\alpha_4 + \xi_2\xi_3\alpha_5 + \xi_1\xi_2\alpha_6$
3	3	$\xi_1\gamma_7 + \xi_2\gamma_8 + \xi_1\xi_2\gamma_9$	$\xi_3\alpha_7 + \xi_2\xi_3\alpha_8 + \xi_1\xi_3\alpha_9$
1	2	$\xi_3\gamma_{10}$	0
2	3	$\xi_1\gamma_{11}$	0
1	3	$\xi_2\gamma_{12}$	0

In both cases the minimum number of parameters needed to obtain proper rank of the mixed formulation are used to define $\mathcal{E}_1(\boldsymbol{\xi}, \cdot)$.

The interpolates for $\tilde{\boldsymbol{\sigma}}$ and $\tilde{\boldsymbol{\varepsilon}}$ in the physical space are obtained by equating (3.7) and (3.8), resulting in

$$\begin{aligned} \tilde{\boldsymbol{\sigma}} &= \boldsymbol{\beta}_0 + \boldsymbol{T}\mathcal{E}_1(\boldsymbol{\xi}, \boldsymbol{\beta})\boldsymbol{T}^T \\ \tilde{\boldsymbol{\varepsilon}} &= \boldsymbol{\gamma}_0 + \frac{1}{j}\boldsymbol{T}^{-T}\left[\mathcal{E}_1(\boldsymbol{\xi}, \boldsymbol{\gamma}) + \mathcal{E}_2(\boldsymbol{\xi}, \boldsymbol{\alpha})\right]\boldsymbol{T}^{-1} \end{aligned} \tag{3.10}$$

where the reparameterization of the constant terms is given by

$$\boldsymbol{\beta}_0 = \boldsymbol{T}\widehat{\boldsymbol{\beta}}_0\boldsymbol{T}^T \quad \text{and} \quad \boldsymbol{\gamma}_0 = \boldsymbol{T}^{-T}\widehat{\boldsymbol{\gamma}}_0\boldsymbol{T}^{-1} \ . \tag{3.11}$$

Remark 3.3.

1. Note the enhanced parameters added in Table 3.2 for the normal strain components are chosen such that the resulting strain components are complete polynomials. This is done to provide the necessary equations to enforce the incompressibility constraint without loss of rank for the resulting finite element arrays, see SIMO *et al.*, [1993].

3.2. Mixed-Enhanced Strain Field

By isolating $(2.10)_3$ we may express the element parameters appearing in the mixed-enhanced strain, $\tilde{\boldsymbol{\varepsilon}}$ in terms of the nodal displacement parameters $\widehat{\boldsymbol{u}}^I$. Recall $(2.10)_3$

$$\int_\Omega \mathrm{tr}\ \left[\delta \tilde{\boldsymbol{\sigma}}^T (\boldsymbol{\varepsilon} - \tilde{\boldsymbol{\varepsilon}})\right]\ dV = 0\ . \tag{3.12}$$

Substituting (3.10) into (3.12) and noting (3.9) we arrive at

$$\begin{aligned} \int_\Omega \mathrm{tr}\ \left[\delta \boldsymbol{\beta}_0^T (\boldsymbol{\varepsilon} - \boldsymbol{\gamma}_0)\right]\ dV = 0 \\ \int_\Omega \mathrm{tr}\ \left[\mathcal{E}_1^T(\delta\boldsymbol{\beta}) \left(\boldsymbol{T}^T(\boldsymbol{\varepsilon} - \boldsymbol{\gamma}_0)\boldsymbol{T} - \frac{1}{j}\mathcal{E}_1(\boldsymbol{\gamma})\right)\right]\ dV = 0\ . \end{aligned} \tag{3.13}$$

Since $\delta\boldsymbol{\beta}_0$ and $\delta\boldsymbol{\beta}$ are independent of the arguments within the integrand and the limits of integration we obtain $\boldsymbol{\gamma}_0$ as

$$\gamma_0 = \frac{1}{V}\int_\Omega \boldsymbol{\varepsilon}\ dV := \boldsymbol{\varepsilon}_0 \tag{3.14}$$

and cast $(3.13)_2$ as

$$\int_\Omega \overline{\boldsymbol{E}}_1^T \left(\boldsymbol{E}_3\boldsymbol{u} - \frac{1}{j}\boldsymbol{E}_1\boldsymbol{\gamma}\right)\ dV = 0\ . \tag{3.15}$$

In (3.15) we have defined the following operators which enable a mapping between tensors and matrices

$$\mathcal{E}_1(\boldsymbol{\gamma}) \to \boldsymbol{E}_1\boldsymbol{\gamma}\ ,\quad \mathcal{E}_1(\boldsymbol{\beta}) \to \overline{\boldsymbol{E}}_1\boldsymbol{\beta}\ ,\quad \boldsymbol{T}^T(\boldsymbol{\varepsilon} - \boldsymbol{\varepsilon}_0)\boldsymbol{T} \to \boldsymbol{E}_3\boldsymbol{u}\ . \tag{3.16}$$

For two dimensions

$$\boldsymbol{E}_1 = \begin{bmatrix} \xi_2 & 0 \\ 0 & \xi_1 \\ 0 & 0 \end{bmatrix} \quad \text{and} \quad \overline{\boldsymbol{E}}_1 = \begin{bmatrix} \xi_2 & 0 \\ 0 & \xi_1 \\ 0 & 0 \end{bmatrix}\ . \tag{3.17}$$

Grouping terms in (3.15) and solving for the element parameter $\boldsymbol{\gamma}$ gives

$$\boldsymbol{\gamma} = \boldsymbol{G}^{-1}\boldsymbol{g}\boldsymbol{u} = \boldsymbol{b}\boldsymbol{u} \tag{3.18}$$

where

$$\boldsymbol{g} = \int_\Omega \overline{\boldsymbol{E}}_1^T \boldsymbol{E}_3\ dV \quad \text{and} \quad \boldsymbol{G} = \int_\square \overline{\boldsymbol{E}}_1^T \boldsymbol{E}_1\ d\square\ . \tag{3.19}$$

Using (3.14) and (3.18) we may rewrite $(3.10)_2$ in matrix notation as

$$\tilde{\boldsymbol{\varepsilon}} = \boldsymbol{B}_u(\boldsymbol{\xi})\boldsymbol{u} + \boldsymbol{B}_\alpha(\boldsymbol{\xi})\boldsymbol{\alpha}\ . \tag{3.20}$$

Remark 3.4.

1. Using the interpolations in Table 3.1 and 3.2 results in a diagonal form for $\boldsymbol{G}$. This simplifies the solution of the element parameters $\boldsymbol{\gamma}$ to a set of scalar decoupled equations.
2. Note orthogonality of $\mathcal{E}_1$ and $\mathcal{E}_2$ is assumed by $(3.9)_3$. In Appendix A we present an alternative formulation for constructing $\mathcal{E}_1$ and $\mathcal{E}_2$ which satisfy the orthogonality condition. However, $(3.9)_{1,2}$ may not hold in general.
3. The distinction between $\boldsymbol{E}_1$ and $\overline{\boldsymbol{E}}_1$ arises since the array, $\boldsymbol{E}_1$ associated with the strain will have two's which multiply the shear coefficients (for the three dimensional case).
4. From the condition $(3.9)_2$ the resulting enhanced strain displacement matrix $\boldsymbol{B}_\alpha$ will inherit the same properties provided any operators multiplying it are constant, $\int_\Omega \boldsymbol{B}_\alpha \boldsymbol{A}_0 \; dV = 0$ with $\boldsymbol{A}_0 = \textit{constant}$. Thus the consistency condition or patch test set forth in SIMO & RIFAI, [1990] is satisfied.
5. The stability condition set forth in SIMO & RIFAI, [1990] requires that the conforming and enhanced spaces be independent. This is satisfied by the choice of interpolations found in Tables 3.1 and 3.2, i.e. the mappings are disjoint.

3.3. Variational Stress Recovery

By isolating $(2.10)_2$ we may solve for the element parameters of the mixed stress, $\tilde{\boldsymbol{\sigma}}$. Recall $(2.10)_2$

$$\int_\Omega \delta\tilde{\boldsymbol{\varepsilon}} \cdot (\boldsymbol{\sigma} - \tilde{\boldsymbol{\sigma}}) \; dV = 0 \tag{3.21}$$

where

$$\boldsymbol{\sigma} = \frac{\partial W}{\partial \tilde{\boldsymbol{\varepsilon}}} \tag{3.22}$$

Substituting (3.10) into (3.21) and noting (3.9) we arrive at

$$\begin{gathered} \int_\Omega \operatorname{tr} \left[\delta\boldsymbol{\gamma}_0^T (\boldsymbol{\sigma} - \boldsymbol{\beta}_0)\right] \; dV = 0 \\ \int_\Omega \operatorname{tr} \left[\frac{1}{j}\mathcal{E}_1^T(\delta\boldsymbol{\gamma}) \left(\boldsymbol{T}^{-1}(\boldsymbol{\sigma} - \boldsymbol{\beta}_0)\boldsymbol{T}^{-T} - \mathcal{E}_1(\boldsymbol{\beta})\right)\right] \; dV = 0 \; . \end{gathered} \tag{3.23}$$

Regarding $\delta\boldsymbol{\gamma}_0$ and $\delta\boldsymbol{\gamma}$ as independent of the arguments within the integrand and the limits of integration we may obtain $\boldsymbol{\beta}_0$ as

$$\boldsymbol{\beta}_0 = \frac{1}{V} \int_\Omega \boldsymbol{\sigma} \; dV := \boldsymbol{\sigma}_0 \tag{3.24}$$

and cast $(3.23)_2$ as

$$\int_\Omega \frac{1}{j} \boldsymbol{E}_1^T \left\{ \boldsymbol{E}_5 - \overline{\boldsymbol{E}}_1 \boldsymbol{\beta} \right\} \; dV = 0 \tag{3.25}$$

where we have defined the following operators which enable a mapping between tensors and matrices

$$\boldsymbol{T}^{-1}(\boldsymbol{\sigma}-\boldsymbol{\sigma}_0)\boldsymbol{T}^{-T} \rightarrow \boldsymbol{E}_5 \ . \tag{3.26}$$

Grouping terms in (3.25) and solving for the element parameter $\boldsymbol{\beta}$ gives

$$\boldsymbol{\beta}=\boldsymbol{G}^{-1}\boldsymbol{h} \quad \text{where} \quad \boldsymbol{h}=\int_\Omega \frac{1}{j}\boldsymbol{E}_1^T\boldsymbol{E}_5 \ dV \ . \tag{3.27}$$

The variationally recoverable stress becomes

$$\tilde{\boldsymbol{\sigma}}=\boldsymbol{\beta}_0+\boldsymbol{T}\mathcal{E}_1(\boldsymbol{\xi},\boldsymbol{\beta})\boldsymbol{T}^T \ . \tag{3.28}$$

Remark 3.5.

1. The variational stresses developed above are used for postprocessing only and are not needed for the construction of the residual or tangent.

3.4. Residual and Tangent

By construction, the substitution of (3.20) into (2.7) renders the second term of (2.7) zero, hence we may express a modified functional $\widehat{\Pi}$ as

$$\widehat{\Pi}(\boldsymbol{u},\tilde{\varepsilon})=\int_\Omega W(\tilde{\varepsilon})\ dV+\Pi_{ext}(\boldsymbol{u}) \tag{3.29}$$

The stationary condition of $\widehat{\Pi}$ yields a reduced set of nonlinear equations, which may be expressed as

$$\delta\widehat{\Pi}=\int_\Omega \frac{\partial W}{\partial\tilde{\varepsilon}}:\delta\tilde{\varepsilon}\ dV \quad\Rightarrow\quad \left\{\,\delta\boldsymbol{u}^T \quad \delta\boldsymbol{\alpha}^T\,\right\}\int_\Omega \left\{\begin{matrix}\boldsymbol{B}_u^T\\ \boldsymbol{B}_\alpha^T\end{matrix}\right\}\boldsymbol{\sigma}\ dV \ + \ \delta\Pi_{ext}=0 \tag{3.30}$$

where $\boldsymbol{\sigma}$ is defined in (3.22).

To solve the mixed boundary value problem the above nonlinear equations are linearized and solved by a Newton's method as a sequence of linearized problems. Hence, linearizing (3.30) we obtain

$$d(\delta\widehat{\Pi})=\int_\Omega d\tilde{\varepsilon}:\frac{\partial^2 W}{\partial\tilde{\varepsilon}^2}:\delta\tilde{\varepsilon}\ dV \quad\Rightarrow\quad \left\{\,\delta\boldsymbol{u}^T \quad \delta\boldsymbol{\alpha}^T\,\right\}\int_\Omega \begin{bmatrix}\boldsymbol{K}_{uu} & \boldsymbol{K}_{u\alpha}\\ \boldsymbol{K}_{\alpha u} & \boldsymbol{K}_{\alpha\alpha}\end{bmatrix} dV \left\{\begin{matrix}d\boldsymbol{u}\\ d\boldsymbol{\alpha}\end{matrix}\right\} \tag{3.31}$$

where

$$\begin{aligned}\boldsymbol{K}_{uu}&=\boldsymbol{B}_u^T\ \mathrm{D}\ \boldsymbol{B}_u\ , &\quad \boldsymbol{K}_{u\alpha}&=\boldsymbol{B}_u^T\ \mathrm{D}\ \boldsymbol{B}_\alpha\\ \boldsymbol{K}_{\alpha u}&=\boldsymbol{K}_{u\alpha}^T\ , & \boldsymbol{K}_{\alpha\alpha}&=\boldsymbol{B}_\alpha^T\ \mathrm{D}\ \boldsymbol{B}_\alpha\end{aligned} \qquad \text{and} \qquad \mathrm{D}=\frac{\partial^2 W}{\partial\tilde{\varepsilon}\partial\tilde{\varepsilon}}\ .$$

Noting that the variations $\delta\boldsymbol{u}$ and $\delta\boldsymbol{\alpha}$ in (3.30) are arbitrary we obtain the finite element residual vectors

$$\begin{gathered}\mathop{\mathsf{A}}_{e=1}^{nelm} \left[\boldsymbol{f}_{int}(\boldsymbol{u}_e,\boldsymbol{\alpha}_e) - \boldsymbol{f}_{ext}(\boldsymbol{u}_e)\right] = \boldsymbol{0} \\ \boldsymbol{f}_{enh}(\boldsymbol{u}_e,\boldsymbol{\alpha}_e) = \boldsymbol{0}, \quad (e = 1, 2, \ldots, nelm)\ .\end{gathered} \tag{3.32}$$

where

$$\boldsymbol{f}_{int}(\boldsymbol{u}_e,\boldsymbol{\alpha}_e) = \int_{\Omega_e} \boldsymbol{B}_u^T \boldsymbol{\sigma}\ dV\ , \qquad \boldsymbol{f}_{enh}(\boldsymbol{u}_e,\boldsymbol{\alpha}_e) = \int_{\Omega_e} \boldsymbol{B}_\alpha^T \boldsymbol{\sigma}\ dV \tag{3.33}$$

$\boldsymbol{f}_{ext}$ is the standard external force vector

$$\boldsymbol{f}_{ext}(\widehat{\boldsymbol{u}}_e) = \int_{\Omega_e} \rho_o \boldsymbol{N}^T \boldsymbol{b}\ dV + \int_{\Gamma_e} \boldsymbol{N}^T \bar{\boldsymbol{t}}\ dS \tag{3.34}$$

and A is the standard finite element assembly operator. With the aid of (3.31), linearizing (3.32) about an intermediate state $(\boldsymbol{u}_e^{(k)}, \boldsymbol{\alpha}_e^{(k)})$ yields

$$\begin{aligned} L[\boldsymbol{f}_{int}] &= \boldsymbol{f}_{int}^{(k)} + \boldsymbol{K}_{uu}^{(k)}\ d\boldsymbol{u}_e + \boldsymbol{K}_{u\alpha}^{(k)}\ d\boldsymbol{\alpha}_e \\ L[\boldsymbol{f}_{enh}] &= \boldsymbol{f}_{enh}^{(k)} + \boldsymbol{K}_{\alpha u}^{(k)}\ d\boldsymbol{u}_e + \boldsymbol{K}_{\alpha\alpha}^{(k)}\ d\boldsymbol{\alpha}_e\ . \end{aligned} \tag{3.35}$$

From $(3.32)_2$ we observe that $(3.35)_2$ may be solved at the element level, therefore condensing out $d\boldsymbol{\alpha}_e$

$$d\boldsymbol{\alpha}_e = -\left[\boldsymbol{K}_{\alpha\alpha}^{(k)}\right]^{-1} \left(\boldsymbol{f}_{enh}^{(k)} + \boldsymbol{K}_{\alpha u}^{(k)}\ d\boldsymbol{u}_e\right)\ . \tag{3.36}$$

Substituting (3.36) into $(3.35)_1$ we arrive at an equivalent displacement model involving only the nodal displacement vector at the global level

$$\boldsymbol{K}^{(k)}\ d\boldsymbol{u} = \boldsymbol{R}^{(k)} \tag{3.37}$$

where

$$\begin{aligned} \boldsymbol{K}^{(k)} &= \mathop{\mathsf{A}}_{e=1}^{nelm} \left[\boldsymbol{K}_{uu} - \boldsymbol{K}_{u\alpha}\ \left(\boldsymbol{K}_{\alpha\alpha}\right)^{-1}\ \boldsymbol{K}_{\alpha u}\right]_e^{(k)} \\ \boldsymbol{R}^{(k)} &= \mathop{\mathsf{A}}_{e=1}^{nelm} \left[\boldsymbol{f}^{ext} - \boldsymbol{f}^{int} + \boldsymbol{K}_{u\alpha}\left(\boldsymbol{K}_{\alpha\alpha}\right)^{-1}\ \boldsymbol{f}^{enh}\right]_e^{(k)}\ . \end{aligned}$$

The system (3.37) is solved and then the unknown fields are updated by

$$\begin{aligned} \boldsymbol{u}_e^{(k+1)} &= \boldsymbol{u}_e^{(k)} + d\boldsymbol{u}_e \\ \boldsymbol{\alpha}_e^{(k+1)} &= \boldsymbol{\alpha}_e^{(k)} + d\boldsymbol{\alpha}_e\ . \end{aligned} \tag{3.38}$$

The process is repeated within a particular time step t_n until convergence of the $(k+1)^{th}$ iterate is obtained, the solution is then advanced to the next time step t_{n+1}.

Remark 3.6.

1. For linear elasticity convergence will be obtained in one iteration and the solution is then advanced to the next time increment.
2. To obtain $d\boldsymbol{\alpha}$ in (3.36) one can either recompute the array for each element for each global iterate k or store the arrays associated with the k global iterate. This storage is in addition to any other history needed for the element such as for inelasticity. For three dimensional problems with fine meshes the demand on memory becomes significant.
3. An alternative algorithm, introduced by Simo *et al.*, [1993], for obtaining the element parameters $\boldsymbol{\alpha}$ is outlined in Appendix B which circumvents the large demand on memory and requires storage of only the element parameters, $\boldsymbol{\alpha}$ from the previous global iterate for non-linear elasticity.

4. Numerical Simulations

In this section we investigate the performance of the proposed formulation described above. Specifically, we show the locking free response in the incompressible limit and improved performance in bending dominated problems. To assess the performance of our formulation several representative simulations are presented below in the setting of plane strain and three dimensional linear elasticity. In addition, modifications to include J_2 plasticity and viscoplasticity outlined in Appendix C illustrate the ease of implementation and performance of the present formulation for physically nonlinear materials. Comparisons are made with different element formulations.

The element formulations considered are:

H1 This hexahedral element is a standard eight-node displacement formulation using tri-linear interpolation functions and a standard 8-pt quadrature rule, its two dimensional counterpart is denoted as **Q1**.

H1/E9 This hexahedral element is an enhanced formulation with 9 enhanced modes and utilizes tri-linear interpolation functions and a standard 8-pt quadrature rule, see Simo & Armero, [1992] for further details, its two dimensional counterpart is denoted as **Q1/E4**.

H1/E12 This hexahedral element is an enhanced formulation with 12 enhanced modes and utilizes modified tri-linear interpolation functions and a special 9-pt quadrature rule, see Simo *et al.*, [1993] for further details.

H1/E21 This hexahedral element is an enhanced formulation with 21 enhanced modes and utilizes tri-linear interpolation functions and a standard 8-pt quadrature rule, see Andelfinger, [1992] for further details.

Shell This 4-node quadrilateral shell has 6 degree-of-freedom per node and utilizes standard order quadrature, see Taylor, [1987] for further details.

H1/ME9 The new mixed-enhanced formulation with 9 enhanced modes, standard tri-linear interpolation functions, and standard 8-pt quadrature rule, its two dimensional counterpart is denoted as **Q1/ME2**.

4.1. Eigenvalue Analysis

To appraise the behavior of the elements above in the nearly incompressible limit an eigenvalue analysis for a single finite element is performed. The two configurations considered are depicted in Figure 4.1.1. For both, the assumed mechanical properties are $E = 1$ and $\nu = 0.499999$. Table 4.1.1 and 4.1.2 include only the 18 non-zero eigenvalues, i.e. the 6 rigid body modes are excluded. Values four orders of magnitude greater than the tabulated values are denoted by the ∞ symbol. For a locking-free element only one mode, corresponding to the dilatational mode, should tend toward infinity as $\nu \to 1/2$. If any additional modes tend toward infinity the element will exhibit volumetric locking.

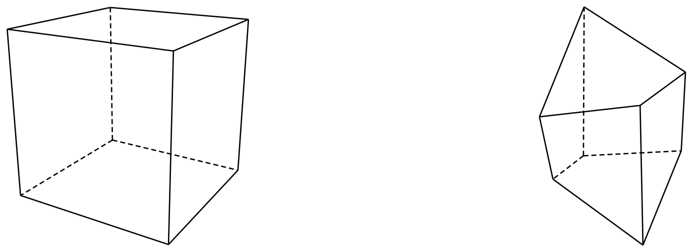

Figure 4.1.1 Undistorted and Distorted Configurations of a Hexahedran

Table 4.1.1 Eigenvalues for a Nearly Incompressible 8-Node Regular Hexahedral Element

Mode	H1	H1/E9	H1/E12	H1/E21	H1/ME9
1	5.5556E-02	5.5556E-02	5.5556E-02	5.5556E-02	5.5556E-02
2	5.5556E-02	5.5556E-02	5.5556E-02	5.5556E-02	5.5556E-02
3	1.6667E-01	1.1111E-01	1.1111E-01	5.5556E-02	5.5556E-02
4	1.6667E-01	1.1111E-01	1.1111E-01	5.5556E-02	5.5556E-02
5	1.6667E-01	1.1111E-01	1.1111E-01	5.5556E-02	5.5556E-02
6	2.2222E-01	2.2222E-01	1.1111E-01	1.1111E-01	1.1111E-01
7	3.3333E-01	3.3333E-01	1.1111E-01	1.1111E-01	1.1111E-01
8	3.3333E-01	3.3333E-01	1.1111E-01	1.1111E-01	1.1111E-01
9	3.3333E-01	3.3333E-01	2.2222E-01	2.2222E-01	2.2222E-01
10	3.3333E-01	3.3333E-01	3.3333E-01	3.3333E-01	3.3333E-01
11	3.3333E-01	3.3333E-01	3.3333E-01	3.3333E-01	3.3333E-01
12	∞	3.3333E-01	3.3333E-01	3.3333E-01	3.3333E-01
13	∞	3.3333E-01	3.3333E-01	3.3333E-01	3.3333E-01
14	∞	3.3333E-01	3.3333E-01	3.3333E-01	3.3333E-01
15	∞	∞	3.3333E-01	3.3333E-01	3.3333E-01
16	∞	∞	3.3333E-01	3.3333E-01	3.3333E-01
17	∞	∞	3.3333E-01	3.3333E-01	3.3333E-01
18	∞	∞	∞	∞	∞

Table 4.1.2 Eigenvalues for Nearly Incompressible 8-Node Distorted Hexahedral Element

Mode	H1	H1/E9	H1/E12	H1/ME9
1	3.6273E-02	3.0720E-02	3.3857E-02	3.3108E-02
2	7.5142E-02	5.5337E-02	5.6785E-02	3.9517E-02
3	1.3489E-01	1.0233E-01	8.0446E-02	6.6768E-02
4	1.6698E-01	1.3401E-01	1.0274E-01	7.4400E-02
5	1.9041E-01	1.4662E-01	1.0760E-01	8.2449E-02
6	2.1365E-01	1.9201E-01	1.2176E-01	8.9910E-02
7	2.5897E-01	2.1791E-01	1.3636E-01	1.0429E-01
8	3.2395E-01	2.5554E-01	1.4528E-01	1.5998E-01
9	3.8442E-01	2.9852E-01	1.8486E-01	1.7127E-01
10	4.0333E-01	3.1738E-01	2.3426E-01	2.2994E-01
11	2.1370E+01	3.8075E-01	2.6414E-01	2.6744E-01
12	∞	4.3302E-01	2.9215E-01	3.0429E-01
13	∞	4.8680E-01	3.4335E-01	3.1834E-01
14	∞	3.8748E+01	3.7548E-01	3.4756E-01
15	∞	∞	3.8995E-01	4.2667E-01
16	∞	∞	4.6811E-01	4.4534E-01
17	∞	∞	5.2791E-01	5.0957E-01
18	∞	∞	∞	∞

4.2. Cook's Membrane Problem

To demonstrate the performance of the proposed element in a bending dominated response, we consider a tapered panel clamped on one end and subjected to an in-plane shearing load on the free end, see Figure 4.2.1. In the context of linear elasticity, this simulation is commonly referred to as Cook's membrane problem. The material properties are taken to be $E = 250$ and $\nu = 0.4999$ such that a nearly incompressible response is effectively obtained.

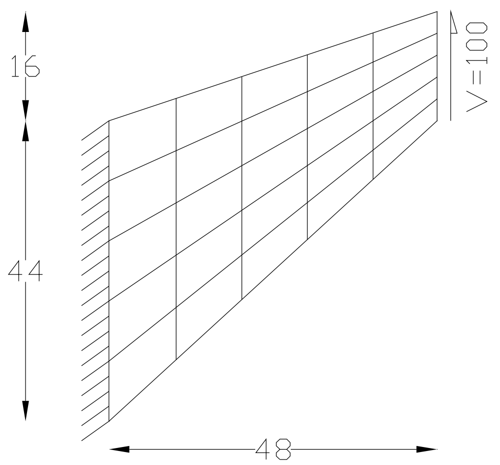

Figure 4.2.1 Cook's Membrane Problem.

In Figure 4.2.2 the top corner vertical displacement is plotted versus number of elements per side. Both the proposed Q1/ME2 element and the Q1/E4 element converge rapidly and show excellent performance, while the standard Q1 element exhibits locking behavior.

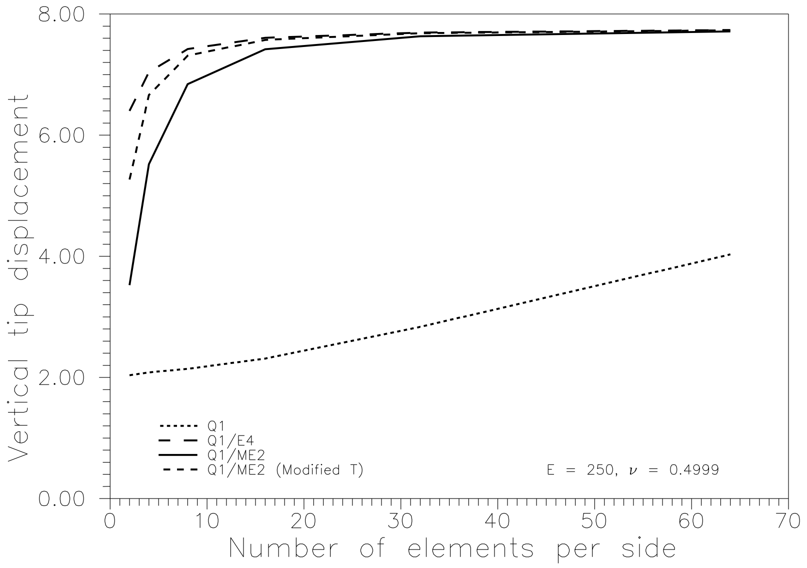

Figure 4.2.2 Convergence of the finite element solutions for Cook's problem.

The dashed line denoted by Q1/ME2 (Modified T) corresponds to modifications made to the average Jacobian $\boldsymbol{T}$ presented in Section 3.1.1. The modifications consist of altering the original reference coordinate system used to compute $\boldsymbol{T}$ by simply rotating the physical element to align equally with the isoparametric coordinate system, while maintaining the aspect ratio. The new coordinate frame is then used to form the average Jacobian. The basic concept is depicted in Figure 4.2.3. This modified Jacobian has two features: a) the proposed Jacobian removes any element distortion, b) and the resulting Jacobian is diagonal yielding additional efficiency for the computation of arrays.

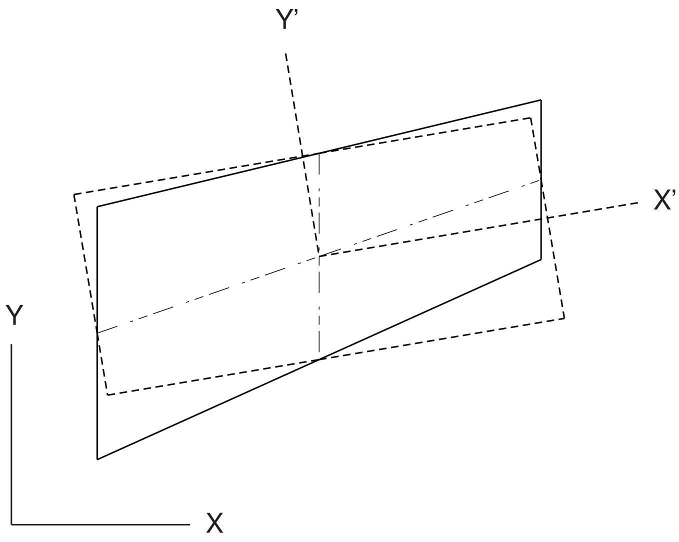

Figure 4.2.3 Rotated reference frame for computation of the average Jacobian.

The solution time reported for both the Q1/ME2 and Q1/E4 methods were approximately the same. Also the convergence of the Q1/ME2 with respect to the energy norm was similar to the Q1/E4.

4.3. Thick Wall Cylinder Problem

To assess the performance of our formulation for a confined nearly incompressible state we consider a thick-walled cylindrical tube. The model consists of a 5° segment of the cylinder as depicted in Figure 4.3.1, with an inner radius $r_i = 7$ and outer radius $r_o = 10$ subjected to an internal pressure $p = 72/(r_i\pi)$. The elastic modulus was taken as $E = 250$, while various values for Poisson's ratio are listed in Table 4.3.1. Further we assume plane strain in the axial direction. Normalized radial displacements with respect to the exact solution are found in Table 4.3.1. Both the Q1/ME2 and Q1/E4 show excellent performance, while the Q1 element locks. The same pattern with respect to solution time and convergence was observed for the present simulation as in the Cook's problem.

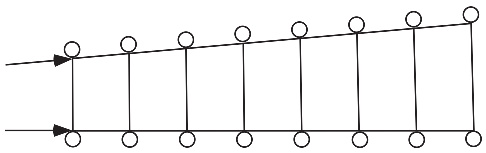

Figure 4.3.1 Thick Wall Cylinder Problem

Table 4.3.1 Normalized Radial Displacement at $r = 10$

ν	Q1	Q1/E4	Q1/ME2
0.49000	1.008	1.014	1.014
0.49900	0.948	1.002	1.002
0.49990	0.638	1.001	1.001
0.49999	0.150	1.001	1.001

4.4. Thick Wall Sphere Problem

To demonstrate the performance of our 3D formulation for a nearly incompressible state in a three-dimensional stress state we consider a thick-walled sphere depicted in Figure 4.4.1 with an inner radius $r_i = 7.5$ and outer radius $r_o = 10$ subjected to an internal pressure $p = 1$. The elastic modulus was taken as $E = 250$, while various values for Poisson's ratio are listed in Table 4.4.1. Normalized radial displacements with respect to the exact solution are found in Table 4.4.1. The H1/ME9 element shows excellent performance, while the H1 element performance is poor and locks. Again the same pattern with respect to solution time and convergence as reported in the previous problems was observed for the present simulation.

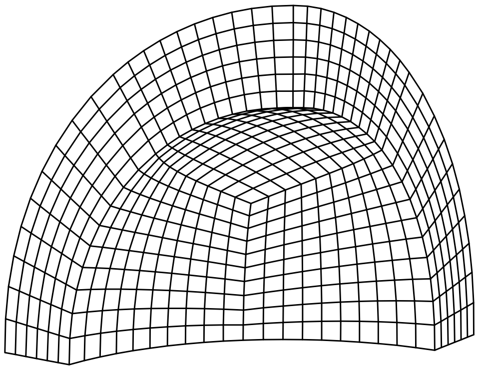

Figure 4.4.1 Thick Wall Sphere Problem

Table 4.4.1 Normalized Radial Displacement at $r = 10$

ν	H1	H1/E9	H1/ME9
0.49000	0.992	1.018	1.019
0.49900	0.772	0.998	1.001
0.49990	0.250	0.985	0.999
0.49999	0.033	0.936	0.999

4.5. Two Dimensional Limit Analysis

To appraise the behavior of the elements above in a highly constrained elastoplastic problem, we introduce the double notched specimen after NAGTEGAAL *et al.*, [1974]. This simulation produces a limit load in terms of the net stress given analytically by $\sigma_{lim} = (2 + \pi)\sigma_y/\sqrt{(3)} \approx 2.97$. The material parameters used for the elastic-perfectly plastic plane strain simulation are: $E = 70$, $\nu = 0.3$ and $\sigma_y = 1.0$, while the geometric properties are: $H = 30$, $W = 10$ and $b = 1$. Due to symmetry only one-quarter of the geometry was analyzed with the resultant mesh being 15×5. The loading was simulated via displacement control at the end opposite the ligament. Thirty displacement increments were chosen for the simulation. Results in Figure 4.5.1 show that the standard displacement formulation does not obtain the limit load, but instead increases monotonically with increased load, whereas the proposed mixed-enhanced formulation asymptotes to near the analytical solution.

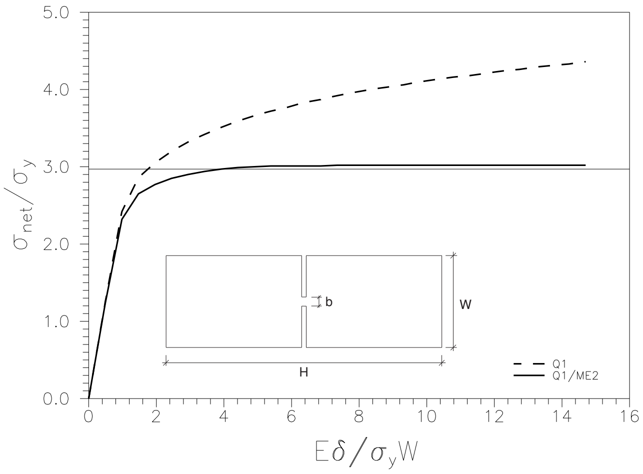

Figure 4.5.1 Notched Tensile Specimen: Limit Analysis

4.6. Three Dimensional Limit Analysis

To appraise the three dimensional behavior of the elements above in a highly constrained elastoplastic problem, we introduce the three dimensional rectangular block after ANDELFINGER *et al.*, [1992]. The material parameters used for the elastic-plastic simulation are: $E = 210,000$, $\nu = 0.3$, $H_{iso} = 210$, $H_{kin} = 0$ and $\sigma_y = 250$, while the geometric properties are: $H = 50$, $W = 100$ and $L = 100$. Due to symmetry only one-quarter of the geometry was analyzed with the resultant mesh being $5 \times 5 \times 5$. The loading was simulated via displacement control at the central patch on the mesh, as depicted in Figure 4.6.1 Thirty displacement increments were chosen for the simulation. Results in Figure 4.6.2 show that the standard displacement formulation does not obtain the limit load, but instead increases monotonically with increased load, whereas the proposed mixed-enhanced formulation asymptotes to the slope of the hardening parameter, H_{iso}.

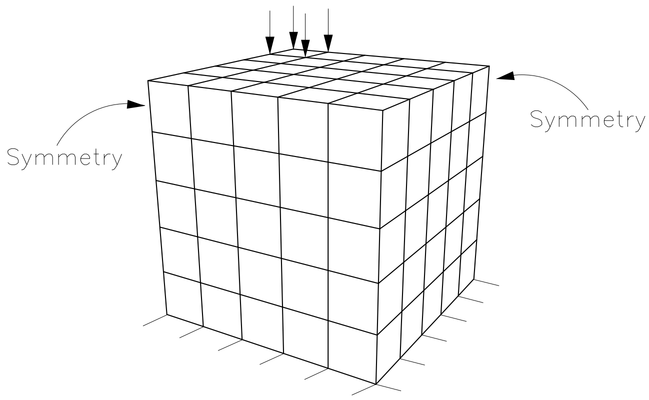

Figure 4.6.1 Elasto-plastic rectangular block

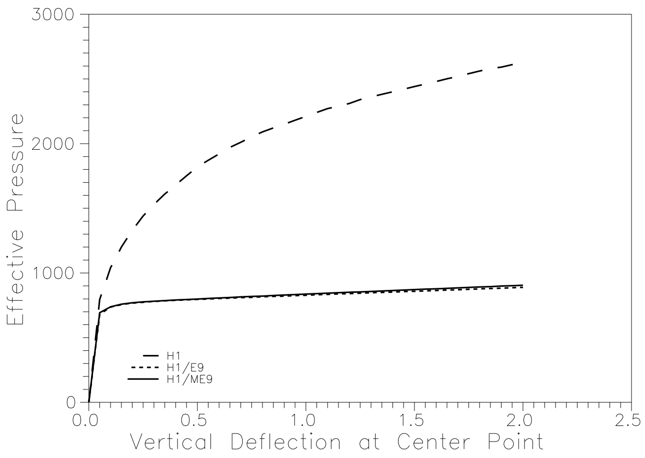

Figure 4.6.2 Load-deflection curves for an elasto-plastic rectangular block

4.7. Viscoplasticity

We consider a perforated strip shown in Figure 4.7.1 illustrating the behavior of the formulation when subject to a viscoplastic response as outlined in Appendix C. The material parameters used for the elastic viscoplastic plane strain simulations are: $E = 70$, $\nu = 0.3$, $\sigma_y = 0.243$, $H_{iso} = 0.135$ and $H_{kiun} = 0.015$ while the geometric properties are: $H = 36$, $W = 10$ and $R = 5$ after an example in Zienkiewicz & Taylor, [1991]. Due to symmetry only one-quarter of the geometry was analyzed. The loading was simulated via displacement control at the end opposite the ligament. Fifteen displacement increments were chosen for the simulation. Results in Figure 4.7.1 shows the results for various values of viscosity as well as the elasticity and rate independent plasticity solution.

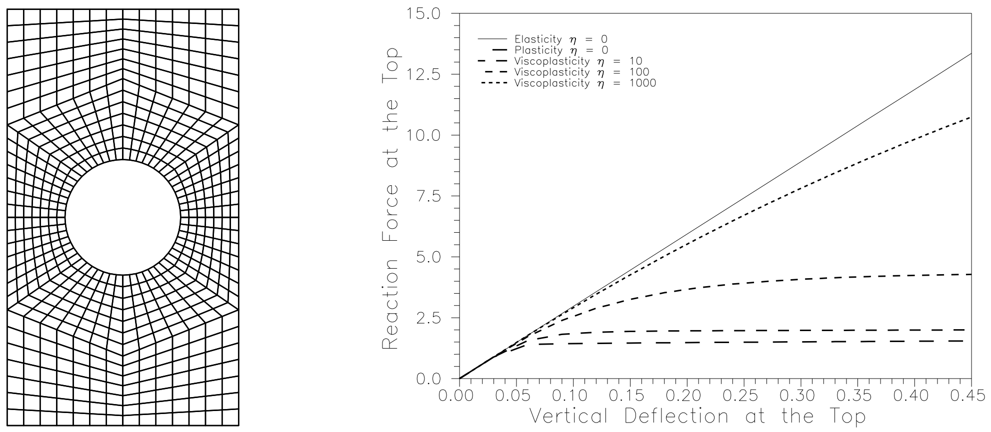

Figure 4.7.1 Perforated Strip at various viscosities

4.8. Pinched Cylindrical Shell with End Diaphragm

To demonstrate the performance of our 3D formulation for singly curved thin shell structures we examine a pinched cylindrical shell with end diaphragm proposed by MacNeal & Harder,[1985]. We consider the configuration of the cylindrical shell as depicted in Figure 4.8.1 with an inner radius $r_i = 300$, wall thickness $t = 3.0$ and length $L = 600$. The elastic modulus was taken as $E = 3.0 \times 10^6$ and a Poisson's ratio of $\nu = 0.3$. One eighth of the shell is modeled by an $N \times N$ mesh defined in cylindrical coordinates. Results reported in Table 4.8.1. for the vertical displacement under the load are normalized with respect to the reference value 1.82488×10^5. The H1/ME9 element shows excellent performance for the thin shell limit.

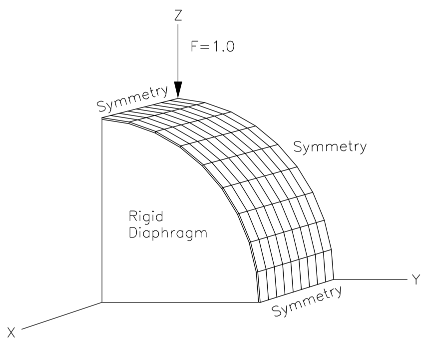

Figure 4.8.1 Pinched Cylindrical Shell Problem

Table 4.8.1 Normalized Displacement under the Load

Mesh	H1	Shell	H1/E9	H1/ME9
$4 \times 4 \times 1$	0.035	0.636	0.081	0.107
$8 \times 8 \times 1$	0.069	0.951	0.405	0.496
$16 \times 16 \times 1$	0.148	1.016	0.838	0.914
$16 \times 16 \times 2$	0.149	-	0.835	0.908
$16 \times 16 \times 3$	0.149	-	0.834	0.907
$32 \times 32 \times 1$	0.315		0.976	0.992

4.9. Pinched Spherical Hemisphere

To demonstrate the performance of our 3D formulation for doubly curved thin shell structures we examine a pinched hemisphere with an open top, modeled as an 18° spherical cap as proposed by MacNeal & Harder,[1985]. We consider the configuration of the spherical shell as depicted in Figure 4.9.1 with an inner radius $r_i = 10$ and wall thickness $t = 0.04$. The elastic modulus was taken as $E = 6.825 \times 10^7$ and a Poisson's ratio of $\nu = 0.3$. One quarter of the shell is modeled by an $N \times N$ mesh defined in spherical coordinates. Results reported in Table 4.9.1. for the displacement under the load are normalized with respect to the reference value 0.094. The H1/ME9 element shows excellent performance for the thin shell limit.

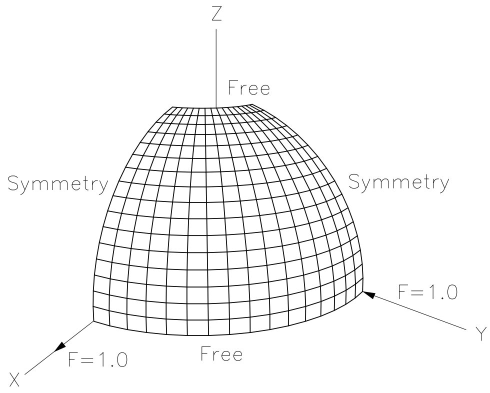

Figure 4.9.1 Pinched Spherical Hemisphere

Table 4.9.1 Normalized Displacement under the Load

Mesh	H1	Shell	H1/E9	H1/ME9
$4 \times 4 \times 1$	0.001	0.897	0.010	0.039
$8 \times 8 \times 1$	0.003	0.999	0.163	0.732
$16 \times 16 \times 1$	0.010	0.995	0.780	0.989
$16 \times 16 \times 2$	0.010	-	0.782	0.988
$16 \times 16 \times 3$	0.010	-	0.749	0.988
$32 \times 32 \times 1$	0.039	0.994	0.974	0.998

5. Closure

We have presented a preliminary investigation for a new class of *assumed strain* methods employing low order finite elements in the setting of physically nonlinear elasticity. The present methodology circumvents difficulties in stress recovery in additional to improved coarse mesh accuracy and locking free response in quasi-incompressible regimes. The formulation exhibits favorable performance in comparison to the Q1/E4 element, which is currently a widely used element.

From the numerical simulations presented, several noteworthy characteristics have been found:

(1) In bending dominated response coarse mesh accuracy is favorable. Improvements to bending dominate regimes may result if: a) introduce alternative enhanced modes, b) introduce alternative procedures (as briefly discussed in Section 4.2) for transforming the isoparametric stress and strain interpolates to the reference configuration. Both classes of improvements need to be pursued in future work.

(2) The orthogonality condition which arises between the stress and enhanced strain field in many *assumed strain* formulations, does not explicitly appear in the present work, hence variationally consistent stress is permissible.

(3) Since the mixed parameters, $\boldsymbol{\gamma}$ may be computed explicitly the resulting element is efficient and retains standard quadrature order to exactly integrate arrays, unlike most enhanced strain formulations.
(4) The element exhibits excellent behavior for configurations where element aspect ratios are large, such as thin shell like structure.
(5) Since the element uses strain driven constitutive relations in the formulation extension to nonlinear constitutive relations is easily obtainable as demonstrated with the implementation of rate dependent and independent plasticity.

The preliminary performance exhibited by the Q1/ME2 and Q1/ME9 in bending and quasi-incompressible regions offers an attractive methodology for a systematic development of mixed-enhanced finite elements. Further extension to finite deformation is currently underway and preliminary results show favorable performance.

References

Andelfinger, U., Ramm, E. & Roehl, D. [1992], "2D- and 3D-Enhanced Assumed Strain Elements and Their Application in Plasticity",*Computational Plasticity, Proceedings of the 4th International Conference,*, ed. D. Owen, E. Onate and E. Hinton, 1997-2007, Pineridge Press, Swansea, U.K.

Korelc, J & Wriggers, P. [1996], "An Efficient 3D Enhanced Strain Element with Taylor Expansion of the Shape Functions", *Computational Mechanics*, **19**, 30-40.

Korelc, J & Wriggers, P. [1997], "Improved Enhanced Strain Four-Node Element with Taylor Expansion of the Shape Functions", *International Journal of Numerical Methods in Engineering*, **40**, 407-421.

Mac Neal, R.H. & Harder, R.L. [1985], "A Proposed Standard Set of Problems to Test Finite Element Accuracy",*Journal of Finite Elements in Analysis and Design*, **1**, 3-20.

Nagtegall, J.C., Parks, D.M. & Rice, J.R. [1974], "On Numerical Accurate Finite Element Solutions in the Fully Plastic Range", *Computer Methods in Applied Mechanics and Engineering*, **4**, 153-177.

Perzyna, P. [1966], "Fundamental Problems in Viscoplasticity", *Advances in Applied Mechanics*, **9**, 243-377.

Simo, J.C. & Rifai, M.S. [1990], "A Class of Mixed Assumed Strain Methods and The Method of Incompatible Modes", *International Journal of Numerical Methods in Engineering*, **29**, 1595-1638.

Simo, J.C. & Armero, F. [1992], "Geometrically Non-linear Enhanced Strain Mixed Methods and the Method of Incompatible Modes", *International Journal of Numerical Methods in Engineering*, **33**, 1413-1449.

Simo, J.C., Armero, F. & Taylor, R.L. [1993], "Improved Versions of Assumed Enhanced Strain Tri-linear Elements for 3D Finite Deformation Problems", *Computer Methods in Applied Mechanics and Engineering*, **110**, 359-386.

Sokolnikoff, I.S. [1964], *Tensor Analysis Theory and Applications to Geometry and Mechanics of Continua*, John Wiley & Sons, Inc., New York.

Taylor, R.L., Beresford, P.J. & Wilson, E.L. [1976], "A Non-Conforming Element for Stress Analysis", *International Journal of Numerical Methods in Engineering*, **10**, 1211-1219.

Taylor, R.L. [1987], "Finite Element Analysis of Linear Shell Problems", *The Mathematics of Finite Elements and Applications VI*, MAFELAP 1987, ed. J.R. Whiteman, Academic Press Limited, London

Washizu, K. [1982], *Variational Methods in Elasticity and Plasticity, 3rd ed.*, Pergamon Press.

Weissman, S.L. [1996], "High-Accuracy Low-Order Three-Dimensional Brick Elements", *International Journal of Numerical Methods in Engineering*, **39**, 2337-2361.

Wilson, E.L., Taylor, R.L., Doherty, W.P. & Ghaboussi, J. [1973], "Incompatible Displacement Models", *Numerical and Computer Methods in Structural Mechanics*, 43.

Zienkiewicz, O.C. & Taylor, R.L. [1991], "The Finite Element Method, Vol 2.", 4th ed., McGraw-Hill.

Appendix A

To allow for general mappings $\mathcal{E}_1$ and $\mathcal{E}_2$ which retain the orthogonality property

$$\int_{\square} \mathcal{E}_1(\cdot)\mathcal{E}_2(\cdot)\ d\square = 0 \tag{A1}$$

we introduce the following transformation

$$\overline{\mathcal{E}}_2(\boldsymbol{\alpha}) = \mathcal{E}_2(\boldsymbol{\alpha}) - \mathcal{E}_1(\boldsymbol{\gamma})\boldsymbol{H}_\gamma^{-1}\boldsymbol{H}_\alpha \tag{A2}$$

where

$$\boldsymbol{H}_\gamma = \int_\Omega \mathcal{E}_1^T(\delta\boldsymbol{\beta})\mathcal{E}_1(\boldsymbol{\gamma})\ dV \quad \text{and} \quad \boldsymbol{H}_\alpha = \int_\Omega \mathcal{E}_1^T(\delta\boldsymbol{\beta})\mathcal{E}_2(\boldsymbol{\alpha})\ dV\ . \tag{A3}$$

Note that the above transformation does not guarantee

$$\int_\square \mathcal{E}_1(\cdot)\ d\square = 0 \quad \text{and} \quad \int_\square \mathcal{E}_2(\cdot)\ d\square = 0 \tag{A4}$$

which allows the element parameters to be easily decoupled. To ensure the resulting arrays are not singular the choice of $\mathcal{E}_1$ and $\mathcal{E}_2$ is such that their columns are linearly independent (i.e. $\boldsymbol{H}_\gamma^{-1}$ exists).

Appendix B

In this appendix we discuss two procedures for the static condensation of the enhanced parameters. Recall $(3.32)_2$ affords a solution of the element parameters $\boldsymbol{\alpha}$ at the element level, thereby obtaining an equivalent displacement model at the global level. This methodology is efficient since additional global equations are not introduced and array sizes remain the same as the Galerkin finite element formulation, which lends itself to simple modification of existing elements.

The first method for obtaining the element parameters, $\boldsymbol{\alpha}$, is the one outlined in Section 3.4 and is outlined in detail below. Accordingly, for a particular time step, t_n, we have the state at the global Newton iterate (k), hence we may construct the following arrays:

$$\begin{aligned}
\boldsymbol{K}_{\alpha\alpha} &= \int_{\Omega_e} \boldsymbol{B}_\alpha^T\ \mathrm{D}(\boldsymbol{u}^{(k)}, \boldsymbol{\alpha}^{(k)})\ \boldsymbol{B}_\alpha\ dV \\
\boldsymbol{K}_{u\alpha} &= \int_{\Omega_e} \boldsymbol{B}_u^T\ \mathrm{D}(\boldsymbol{u}^{(k)}, \boldsymbol{\alpha}^{(k)})\ \boldsymbol{B}_\alpha\ dV \\
\boldsymbol{f}_{enh} &= \int_{\Omega_e} \boldsymbol{B}_\alpha^T \boldsymbol{\sigma}(\boldsymbol{u}^{(k)}, \boldsymbol{\alpha}^{(k)})\ dV\ .
\end{aligned} \tag{B5}$$

These arrays are then used to form the modified tangent and residual

$$\begin{aligned}
\boldsymbol{K}^{(k)} &= \Big[\boldsymbol{K}_{uu} - \boldsymbol{K}_{u\alpha}\ \left(\boldsymbol{K}_{\alpha\alpha}\right)^{-1}\ \boldsymbol{K}_{\alpha u}\Big]_e^{(k)} \\
\boldsymbol{R}^{(k)} &= \Big[\boldsymbol{f}_{ext} - \boldsymbol{f}_{int} + \boldsymbol{K}_{u\alpha}\left(\boldsymbol{K}_{\alpha\alpha}\right)^{-1}\ \boldsymbol{f}^{enh}\Big]_e^{(k)}\ .
\end{aligned} \tag{B6}$$

The modified element arrays are then assembled into global arrays

$$\mathop{\mathbf{A}}_{e=1}^{nelm} \boldsymbol{K}^{(k)} d\boldsymbol{u}^{(k+1)} = \mathop{\mathbf{A}}_{e=1}^{nelm} \boldsymbol{R}^{(k)} \tag{B7}$$

which may be solved for the incremental nodal displacement vector, $d\boldsymbol{u}$ and then used to update the nodal displacement vector

$$\boldsymbol{u}^{(k+1)} = \boldsymbol{u}^{(k)} + d\boldsymbol{u}^{(k+1)}\ . \tag{B8}$$

The incremental displacements may be substituted into the expression for the increment of the element parameters

$$d\boldsymbol{\alpha}^{(k+1)} = -\left[\boldsymbol{K}_{\alpha\alpha}^{(k)}\right]^{-1}\left(\boldsymbol{f}_{enh}^{(k)} + \boldsymbol{K}_{\alpha u}^{(k)}\; d\boldsymbol{u}^{(k+1)}\right) \tag{B9}$$

which then may be used to update the element parameters

$$\boldsymbol{\alpha}^{(k+1)} = \boldsymbol{\alpha}^{(k)} + d\boldsymbol{\alpha}^{(k+1)} \; . \tag{B10}$$

Note (B9) and (B10) can not be performed until the global system is assembled and the state $d\boldsymbol{u}^{(k+1)}$ found. This necessitates saving the arrays (B5) for subsequent use in updating the element parameters, in additional to any existing arrays (i.e. plastic strains, etc.), to reduce unnecessary recomputation of the arrays for each iterate. This storage places significant demands on memory or disk especially for 3D problems which can be substantial for fine meshes. An alternative procedure set forth in SIMO *et al.*, [1993] reduces the required storage to only the current values of the element parameters and is discussed next.

The alternative algorithm proposed in SIMO *et al.*, [1993] is obtained by linearizing the enhanced residual $(3.32)_2$ with respect to $\boldsymbol{\alpha}$ only. Accordingly, we obtain

$$L[\boldsymbol{f}_{enh}] = \boldsymbol{f}_{enh} + \boldsymbol{K}_{\alpha\alpha}\; d\boldsymbol{\alpha} \quad \Rightarrow \quad d\boldsymbol{\alpha} = -\left[\boldsymbol{K}_{\alpha\alpha}\right]^{-1} \boldsymbol{f}_{enh} \; . \tag{B11}$$

The algorithm is outlined as follows for a particular time step, t_n, global Newton iterate (k) and local Newton iterate (i)

1. Initialize index and element parameters for each element
   $i = 0$
   $\boldsymbol{\alpha}^{(i,k)} = \boldsymbol{\alpha}^{(k-1)}$
2. Form enhanced strain displacement matrix
   $\boldsymbol{B}_\alpha^T$
3. Form enhanced tangent matrix
   $\boldsymbol{K}_{\alpha\alpha}^{(i,k)} = \int_{\Omega_e} \boldsymbol{B}_\alpha^T\, \mathrm{D}(\boldsymbol{u}^{(k)}, \boldsymbol{\alpha}^{(i,k)})\; \boldsymbol{B}_\alpha \; dV$
4. Compute enhanced residual
   $\boldsymbol{f}_{enh}^{(i,k)} = \int_{\Omega_e} \boldsymbol{B}_\alpha^T \boldsymbol{\sigma}(\boldsymbol{u}^{(k)}, \boldsymbol{\alpha}^{(i,k)})\; dV$
5. Locally solve for the enhanced increments for each element
   $d\boldsymbol{\alpha}^{(i+1,k)} = -\left[\boldsymbol{K}_{\alpha\alpha}^{(i,k)}\right]^{-1} \boldsymbol{f}_{enh}^{(i,k)}$
6. Local update for the element parameters
   $\boldsymbol{\alpha}^{(i+1,k)} = \boldsymbol{\alpha}^{(i,k)} + d\boldsymbol{\alpha}^{(i+1,k)}$
7. Check for convergence
   `IF (converged) THEN`
     $\boldsymbol{\alpha}^{(k)} = \boldsymbol{\alpha}^{(i+1,k)}$

```
  EXIT
ELSE
  i ← i + 1
  GOTO 3      for physical material nonlinearities
  GOTO 4      for linear elasticity
END IF
```

Appendix C

A General Formulation for Rate Dependent Plasticity

We shall consider a linearized theory of rate-dependent plasticity after PERZYNA, [1966], in which all relevant quantities needed within the theory are infinitesimal to the first order and the loading criteria is relative to stress space. In addition to the infinitesimal strain measure ε_{ij}, we assume the existence of a symmetric plastic strain measure ε^p_{ij} and a measure of work hardening specified by the scalar function κ. From the former we additively define an elastic strain tensor as

$$\varepsilon^e_{ij} = \varepsilon_{ij} - \varepsilon^p_{ij} \; . \tag{C12}$$

We also admit the existence of a scalar valued function $F(\sigma_{ij}, \varepsilon^p_{ij})$ called the static yield function, which is continuously differentiable with respect to its arguments, convex and satisfies the equality

$$F(\sigma_{ij}, \varepsilon^p_{ij}) = \frac{f(\sigma_{ij}, \varepsilon^p_{ij})}{\kappa} - 1 \tag{C13}$$

where $f(\sigma_{ij}, \varepsilon^p_{ij})$ is termed the dynamical yield function. Note for $F = 0$ and fixed values of ε^p_{ij} and κ, (C13) describes a orientable hypersurface of dimension five in six dimensional stress space from which an elastic domain is defined for $F < 0$ and a plastic domain for $F \geq 0$.

For the materials under consideration, attention is restricted to initially homogeneous and isotropic materials where the elastic region is independent of any viscous effects. Following (C12) the strain rate may also be additively decomposed into elastic and plastic parts

$$\dot{\varepsilon}_{ij} = \dot{\varepsilon}^e_{ij} + \dot{\varepsilon}^p_{ij} \tag{C14}$$

where $\dot{\varepsilon}^p_{ij}$ includes both viscous and plastic effects and the superposed dot stands for the material time derivative with respect to t holding $\mathbf{X}$ fixed. The elastic-plastic response of the material may be characterized by a suitable choice of constitution for each of the independent variables. The stress response for σ_{ij} is characterized by the following constitutive relation for generalized Hooke's law

$$\sigma_{ij} = \bar{s}\,\delta_{ij} + \tau_{ij} \tag{C15}$$

where

$$\tau_{ij} = 2\mu\varepsilon^e_{ij} \quad \text{and} \quad \bar{s} = 3k\varepsilon^e_{kk}$$

represent the deviatoric and spherical components of the stress tensor σ_{ij} and μ and k are the shear and bulk modulus, respectfully. The plastic strain rate is given by the constitutive form

$$\dot{\varepsilon}_{ij}^{p} = \begin{cases} 0 & \text{for } F < 0 \\ \gamma\Phi(F)\frac{\partial f}{\partial \sigma_{ij}} & \text{for } F \geq 0 \end{cases} \tag{C16}$$

where γ denotes a viscosity constant of the material and $\Phi(F)$ is commonly taken as $\Phi(F) = F^m$ where m is some positive integer. While the work hardening is proportional to the total plastic work

$$\kappa = \bar{\kappa} \int_0^{\boldsymbol{\varepsilon}^P} \sigma_{ij}\; d\varepsilon_{ij}^{p} \ . \tag{C17}$$

Substituting (C15) and (C16) into (C14) we obtain an expression for the strain rate during loading

$$\dot{\varepsilon}_{ij} = \frac{1}{2\mu}\dot{\sigma}_{ij} + \frac{1}{3k}\dot{\bar{s}}\;\delta_{ij} + \gamma\Phi(F)\frac{\partial f}{\partial \sigma_{ij}} \ . \tag{C18}$$

Taking the inner product of both sides of (C16) with itself we obtain a measure of the magnitude of the plastic strain rate as

$$\bar{e}^p = \left(\dot{\varepsilon}_{ij}^{p}\dot{\varepsilon}_{ij}^{p}\right)^{\frac{1}{2}} = \gamma\Phi(F)\left(\frac{\partial f}{\partial \sigma_{ij}}\frac{\partial f}{\partial \sigma_{ij}}\right)^{\frac{1}{2}} \ . \tag{C19}$$

Substituting (C19) into (C13) we obtain an expression for the dynamical yield function

$$f(\sigma_{ij}, \varepsilon_{ij}^{p}) = \kappa\left\{1 + \left[\frac{\bar{e}^p}{\gamma}\left(\frac{\partial f}{\partial \sigma_{ij}}\frac{\partial f}{\partial \sigma_{ij}}\right)^{-\frac{1}{2}}\right]^{-m}\right\} \tag{C20}$$

for $\Phi(F) = F^m$ which shows the dependency of the yield function on the strain rate.

Numerical Formulation

We shall now consider the special form $\Phi(F) = F$ for the numerical implementation of the plastic/viscoplastic model. From (C16) we see that the plastic strain rate now has the form

$$\dot{\varepsilon}_{ij}^{P} = \gamma F\frac{\partial f}{\partial \sigma_{ij}} \tag{C21}$$

upon loading. Recall for classical rate independent theory the plastic strain rate is given by

$$\dot{\varepsilon}_{ij}^{P} = \dot{\lambda}\frac{\partial f}{\partial \sigma_{ij}} \tag{C22}$$

where $\dot{\lambda}$ is called the plastic consistency parameter. Equating (C21) and (C22) we obtain the yield criteria as

$$\gamma F - \dot{\lambda} = 0 \ . \tag{C23}$$

In the current work the scalar valued function F will take a von Mises type form given by

$$F = \sqrt{(\tau_{ij} - \alpha_{ij})(\tau_{ij} - \alpha_{ij})} - \kappa \tag{C24}$$

where τ is the deviatoric stress, α is a deviatoric back stress allowing for translations of the yield surface and κ a scalar valued work hardening function allowing for expansion of the yield surface. The quantities α and κ are commonly referred to as *kinematic* and *isotropic* hardening parameters. Using the assumed Mises form we may rewrite the yield criteria as

$$\sqrt{(\tau_{ij} - \alpha_{ij})(\tau_{ij} - \alpha_{ij})} - \kappa - \frac{1}{\gamma}\dot{\lambda} = 0 \; . \tag{C25}$$

The constitutive equation for the back stress following Zienkiewicz, *et al.*, [1991], will be given in terms of the back stress rate $\dot{\alpha}_{ij}$ which is taken proportional to the plastic strain rate as

$$\dot{\alpha}_{ij} = \frac{2}{3} H_{kin} \dot{\varepsilon}^p_{ij} \tag{C26}$$

where H_{kin} is a measure of the translation of the yield surface. While the work hardening parameter is given as a measure of the magnitude of the plastic strain rate and the initial yield

$$\kappa = \sigma_{yo} + H_{iso} \bar{e}^p \tag{C27}$$

where H_{iso} is a measure of the expansion of the yield surface and $\bar{e}^p$ is the accumulated plastic strain given by

$$\bar{e}^p = \int_0^t \sqrt{\frac{2}{3} \dot{\varepsilon}^p_{ij} \dot{\varepsilon}^p_{ij}} \; d\sigma \; . \tag{C28}$$

Element Formulation

The following modifications will be made to the above mixed-enhanced strain formulation. To include isotropic J_2 plasticity/viscoplasticity with linear isotropic and kinematic hardening to the former formulation the following modifications are made.

1. Compute trial deviatoric stress, ${}^{tr}\boldsymbol{\tau}$, note the ${}^{tr}[\cdot]$ denote trial values to be updated later within the algorithm.

   $${}^{tr}\boldsymbol{\tau}_{n+1} = 2\mu \left(\boldsymbol{\varepsilon}_{n+1} - \boldsymbol{\varepsilon}^p_n \right)$$

   $\boldsymbol{\varepsilon}^p$ is the plastic strain.

2. Compute back stress adjusted value, $\boldsymbol{\Sigma}$

   $${}^{tr}\boldsymbol{\Sigma}_{n+1} = {}^{tr}\boldsymbol{\tau}_{n+1} - \boldsymbol{\alpha}_n$$

3. Compute the radius of the yield function, R

   $$R_{n+1} = \sqrt{\frac{2}{3}} \left(\sigma_{yo} + H_{iso} \bar{e}^p_n \right)$$

4. Compute the norm of the back stress adjusted value, $\| \boldsymbol{\Sigma} \|$

$$\| {}^{tr}\boldsymbol{\Sigma}_{n+1} \| = \sqrt{{}^{tr}\boldsymbol{\Sigma}_{n+1} \cdot {}^{tr}\boldsymbol{\Sigma}_{n+1}}$$

5. Compute consistency parameter, λ

$$\lambda_{n+1} = A \left(\| {}^{tr}\boldsymbol{\Sigma}_{n+1} \| - R_{n+1} \right) / 2\mu$$

$$\text{where} \qquad A = \frac{1}{1 + \frac{1}{3}\left(H_{iso} + H_{kin}\right) + \frac{\eta}{2\mu\Delta t}} \qquad \text{and} \qquad \eta = \frac{1}{\gamma}$$

where Δt is the current time increment.

6. Compute plastic solution state

$$if \ \left(\| \boldsymbol{\Sigma}_{n+1} \| - R_{n+1} > \frac{\eta}{\Delta t}\lambda_{n+1} \right) \ then$$

$$\bar{e}^p_{n+1} = \bar{e}^p_n + \sqrt{\frac{2}{3}}\lambda_{n+1}$$

$$\mathbf{n}_{n+1} = \frac{{}^{tr}\boldsymbol{\Sigma}_{n+1}}{\| {}^{tr}\boldsymbol{\Sigma}_{n+1} \|}$$

$$\boldsymbol{\tau}_{n+1} = {}^{tr}\boldsymbol{\tau}_{n+1} - 2\mu\lambda_{n+1}\mathbf{n}_{n+1}$$

$$\boldsymbol{\alpha}_{n+1} = \boldsymbol{\alpha}_n + \frac{2}{3}H_{kin}\lambda_{n+1}\mathbf{n}_{n+1}$$

$$\boldsymbol{\varepsilon}^p_{n+1} = \boldsymbol{\varepsilon}^p_n + \lambda_{n+1}\mathbf{n}_{n+1}$$

$$C_p = k\mathbf{1} \otimes \mathbf{1} + 2\mu(1 - B)\left[\mathbf{I} - \frac{1}{3}\mathbf{1} \otimes \mathbf{1}\right] + 2\mu(B - A)\mathbf{n} \otimes \mathbf{n}$$

$$\text{where} \qquad B = \frac{2\mu\lambda_{n+1}}{\| \boldsymbol{\Sigma}_{n+1} \|}$$

7. Assemble global tangent and solve, GOTO 1